

ANALYSIS OF STEEL-CONCRETE COMPOSITE FRAMES WITH BOND-SLIP

By M. Reza Salari¹ and Enrico Spacone,² Associate Member, ASCE

ABSTRACT: Recent developments in modeling the slip in steel-concrete composite beams have led to an accurate and numerically stable force-based frame element. The element assumes force fields rather than displacement fields along the element. After a brief review of the element formulation, the paper discusses a new phenomenological law for the shear connection between steel girder and concrete slab that considers stiffness and strength degradation. Correlation studies with available push-pull tests on shear connectors are used to validate the proposed model. The steel-concrete composite frame element is then applied to (1) the study of a composite structural subassemblage for which experimental data are available; and (2) the analysis of a three-story, four-bay steel building with a composite deck. In the first case, good agreement is obtained with the experimental results for both full and partial connection conditions. In the second, the study shows the increase in stiffness and strength due to the composite action. The accuracy of the force-based element leads to the use of one or two elements for a single structural member, thus allowing entire frame analyses to be performed economically.

INTRODUCTION

Several studies have focused in recent years on the nonlinear analysis of steel-concrete composite frames. In the United States, these activities have centered around the National Science Foundation (NSF)-sponsored U.S.-Japan Program on Composite and Hybrid Structures. Studies performed in this framework have led to major advances in the state of the art of modeling of steel-concrete composite frames under monotonic and dynamic loads. The main goals of these endeavors have been to improve current seismic design procedures and to gain a better understanding of the seismic behavior of composite structures using nonlinear analyses. With the emergence of new performance-based design philosophies, nonlinear models should eventually become an integral part of the design process in assessing the performance of composite frames subjected to the design earthquakes.

The availability of efficient, precise, and robust models is of primary importance for performing nonlinear static and dynamic analyses of composite frames. In particular, beam and beam-column models that consider the partial interaction between steel girder and concrete slab are essential to such analyses. Early efforts in this area used displacement-based elements (Amadio and Fragiaco 1993; Daniels and Crisinel 1993), which proved precise only if a large number of elements were used in a single composite member. El-Tawil et al. (1996) developed models for the beam-to-column connections, another very important aspect of the nonlinear response of composite frame, and did not consider the partial interaction in the composite beams. Hajjar et al. (1998) used displacement-based elements to study the effects of slip in concrete-filled steel tubes.

In order to improve the accuracy of available modeling techniques, Salari et al. (1998) proposed a force-based element for composite structures with partial interaction. This approach followed earlier studies that showed that controlling the force rather than the displacement fields along the beam leads to more accurate results in problems with bond slip. The model by Salari et al. (1998) is very accurate, but does not extend to

elements with softening in the girder-to-slab interface caused by failure of the shear stud connections. Ayoub and Filippou (2000) propose a mixed formulation to the problem, where both displacement and force fields are assumed along the beam. Finally, Salari and Spacone (2001) extend the original force-based formulation by Salari et al. (1998) to the fully nonlinear case, with softening due to crushing of the concrete slab and/or failure of the shear connection.

This paper focuses on two aspects of the force-based steel-concrete composite beam element: (1) the development and implementation of a new constitutive law for the shear connectors; and (2) the application of the model to the study of two structural systems: a composite structural subassemblage tested at the University of Trento, Italy, and a steel frame with composite decks. A brief review of the force-based element formulation is presented first, followed by the discussion of the new constitutive law for the shear connection. The new law is validated by comparisons with available push-pull test data on shear stud connectors. The model application to the two structural systems follows, with emphasis on the accuracy of the force-based element and its ease of application to the nonlinear analysis of full structural frames.

FORCE-BASED COMPOSITE BEAM ELEMENT

Fig. 1 shows the geometry, bond force distribution, and nodal forces of the two-node force-based element without rigid body modes. The element without rigid body modes has five degrees of freedom (shown in Fig. 1). In the element with rigid body modes, each mode has four degrees of freedom (one rotation, one vertical displacement, the horizontal displacement in the slab, and that in the beam). The bond force $D_b(x)$

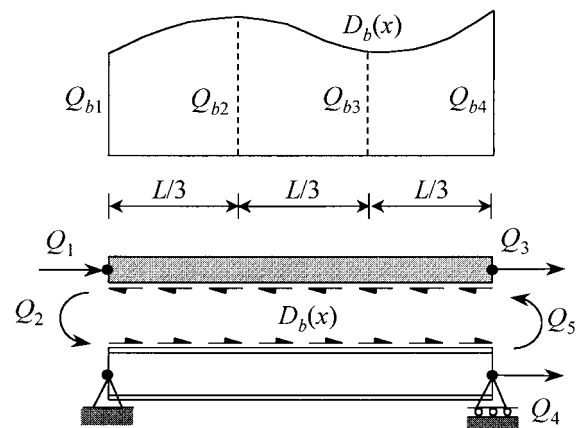


FIG. 1. Force-Based Composite Beam Element

¹Sr. Struct. Engr., RockSol Consulting Group, Inc., 848 Yellow Pine Ave., Boulder, CO 80304.

²Assoc. Prof., Dept. of Civ., Envir., and Arch. Engrg., Univ. of Colorado, Boulder, CO 80309-0428.

Note. Associate Editor: Marc Hoit. Discussion open until April 1, 2002. To extend the closing date one month, a written request must be filed with the ASCE Manager of Journals. The manuscript for this paper was submitted for review and possible publication on September 26, 2000; revised April 23, 2001. This paper is part of the *Journal of Structural Engineering*, Vol. 127, No. 11, November, 2001. ©ASCE, ISSN 0733-9445/01/0011-1243-1250/\$8.00 + \$.50 per page. Paper No. 22574.

along the element is approximated by a cubic function. Other bond distributions were considered, but the cubic distribution was selected because it closely traces the bond distribution in beams with double curvature normally encountered in frames under lateral loads (Salari 1999). The cubic bond distribution results in fourth-order distributions for the bending moment and the axial force along the beam, which can be obtained through element equilibrium. The equilibrium conditions are satisfied pointwise along the element.

Salari et al. (1998) proposed a force-based formulation for the composite beam of Fig. 1. The original formulation is limited to nonsoftening members. More recently, Salari and Spacone (2001) have extended the formulation to comprise any unidimensional problem with bond slip. The main steps of the formulation will be summarized here.

In the force-based element, the internal forces (that is, the bending moment and the axial load) of the main body, \mathbf{s} , and the bond force, \mathbf{s}_b , are interpolated in terms of the element nodal forces \mathbf{Q} and the interface forces \mathbf{Q}_b at selected reference points along the interface. The resulting expression is

$$\begin{Bmatrix} \mathbf{s} \\ \mathbf{s}_b \end{Bmatrix} = \begin{bmatrix} \mathbf{N}_{BB} & \mathbf{N}_{Bb} \\ \mathbf{N}_{bB} & \mathbf{N}_{bb} \end{bmatrix} \begin{Bmatrix} \mathbf{Q} \\ \mathbf{Q}_b \end{Bmatrix} \quad (1)$$

where \mathbf{N}_{BB} , \mathbf{N}_{Bb} , \mathbf{N}_{bB} , and \mathbf{N}_{bb} are the force interpolation functions. Subscript B refers to the main body, and b refers to the bond. Explicit expressions of the above force interpolation functions are found in Salari et al. (1998). Application of the principle of virtual forces leads to the following matrix compatibility relation:

$$\mathbf{F}\Delta\mathbf{Q} = \mathbf{U} - \mathbf{U}_B - \mathbf{U}_b \quad (2)$$

where \mathbf{F} is the element flexibility matrix, given by

$$\mathbf{F} = \mathbf{F}_{BB} - \mathbf{F}_{Bb}(\mathbf{F}_{bb})^{-1}\mathbf{F}_{bB} \quad (3)$$

with

$$\mathbf{F}_{BB} = \int_L (\mathbf{N}_{BB}^T \mathbf{f} \mathbf{N}_{BB} + \mathbf{N}_{bB}^T \mathbf{f}_b \mathbf{N}_{bB}) dx \quad (4a)$$

$$\mathbf{F}_{Bb} = \int_L (\mathbf{N}_{BB}^T \mathbf{f} \mathbf{N}_{Bb} + \mathbf{N}_{bB}^T \mathbf{f}_b \mathbf{N}_{bb}) dx \quad (4b)$$

$$\mathbf{F}_{bB} = \mathbf{F}_{Bb}^T; \quad \mathbf{F}_{bb} = \int_L (\mathbf{N}_{bb}^T \mathbf{f}_b \mathbf{N}_{bb} + \mathbf{N}_{bB}^T \mathbf{f}_b \mathbf{N}_{bB}) dx \quad (4c,d)$$

The main body section flexibility is \mathbf{f} and \mathbf{f}_b is the bond flexibility; \mathbf{U} contains the nodal displacements; and \mathbf{U}_B and \mathbf{U}_b are the contributions of the main body and the bond deformations to the nodal displacements, respectively, and are defined by

$$\mathbf{U}_B = \int_L \{\mathbf{N}_{BB}^T - \mathbf{F}_{Bb}(\mathbf{F}_{bb})^{-1}\mathbf{N}_{bB}^T\} \mathbf{e} dx \quad (5a)$$

$$\mathbf{U}_b = \int_L \{\mathbf{N}_{bb}^T - \mathbf{F}_{bb}(\mathbf{F}_{bb})^{-1}\mathbf{N}_{bb}^T\} \mathbf{e}_b dx \quad (5b)$$

where \mathbf{e} are the beam section deformations (axial strain and curvature) and \mathbf{e}_b is the bond deformation, that is, the slip at the contact points. Slab uplifting is neglected; thus only sliding is considered at the beam-to-slab interface.

In order to use the above formulation in a general-purpose displacement-based finite-element analysis code, two operations are needed: (a) compute the element stiffness matrix \mathbf{K} by inverting the flexibility matrix \mathbf{F} ; and (b) recover the element forces corresponding to the element displacements \mathbf{U} . This second step requires an element state determination algorithm that has evolved from the original scheme by Spacone

et al. (1996), which was developed for a beam with perfect bond, to the scheme presented in Salari and Spacone (2001). The procedure adjusts the element forces until the right-hand side of (2) equals zero; that is, until the element compatibility is satisfied in an integral sense. The procedure maintains pointwise equilibrium between nodal and section forces by enforcing (1). The element formulation has been successfully applied to different classes of elements with bond slip, including a steel rebar embedded in concrete, a reinforced concrete element with bar slip, and a steel-concrete composite frame element.

CYCLIC BOND CONSTITUTIVE LAW

The element formulation relies on the fiber section discretization to compute the section forces and stiffness corresponding to the section deformations \mathbf{e} . The section force-deformation relation is established by integration of the uniaxial stress-strain behavior of the layers (Spacone et al. 1996). The concrete model used in all the numerical studies is that by Kent and Park (1971). The steel nonlinear behavior is described by the Menegotto-Pinto (1973) steel model. As for the law describing the shear stud connection, the initial implementation of the element used the law developed by Elgehausen et al. (1983) for reinforcing bars with bond slip. The law gave satisfactory overall results, but the correlation with available experimental results on shear stud connections was not always good. Also, the law by Elgehausen et al. (1983) has stiffness jumps and has a flat plateau at the peak strength. These characteristics caused numerical problems when combined with the force-based formulation. To circumvent these difficulties, a new law was formulated to compute the shear force corresponding to the slip \mathbf{e}_b . The constitutive law is a uniaxial model that considers the tangent (sliding) component of the bond force only. The model is capable of accounting for the deterioration of the bond strength and stiffness during the load cycles.

A schematic representation of the force-slip relation for a headed shear stud connection is shown in Fig. 2, where u indicates the slip and q the bond force. The stiffness of the ascending branch of the monotonic envelope reduces gradually from the initial value to zero at the ultimate bond force q_1 . Upon passing the peak, the bond strength decreases until the ultimate frictional bond q_{fu} is reached. The cyclic bond behavior is characterized by a steep unloading branch AB, which results in the large inelastic residual deformation OB. As unloading continues, the gap between the shear stud and the concrete and the voids between the concrete particles close. This

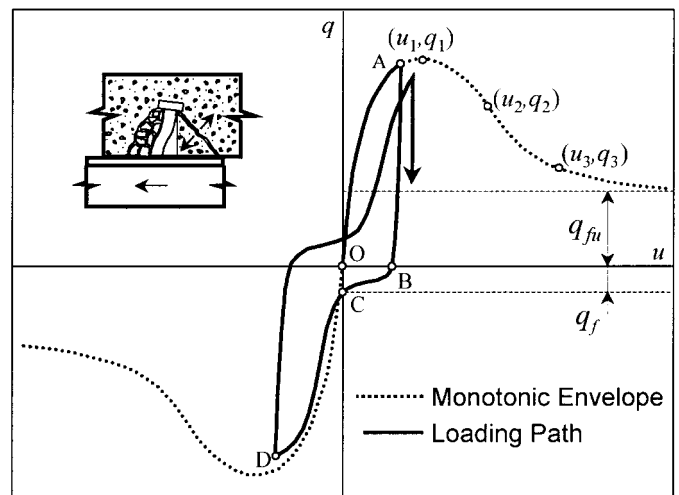


FIG. 2. Cyclic Force-Slip Behavior of Shear Stud Connection

behavior is represented by branch BC, which has a very small stiffness and ends at point C in Fig. 2, with a prescribed bond force of q_f . After the gaps have closed, the bond stiffness quickly increases until the concrete begins crushing on the other side of the shear stud. Bond strength and bond stiffness deteriorate during loading and unloading cycles. The curve CD in Fig. 2 schematically shows the degradation effect on the bond force-slip envelope.

The monotonic envelope of Fig. 2 is divided into two branches:

1. The ascending branch, from the origin to the peak (u_1, q_1), whose equation is

$$q = q_1 \alpha_1 \bar{u} \exp(-\alpha_2 \bar{u}^{\alpha_3}); \quad 0 < \bar{u} < 1 \quad (6a,b)$$

where $\bar{u} = u/u_1$. The three parameters α_1 , α_2 , and α_3 are obtained by enforcing the condition that $q'(0) = E_0$, $q(u_1) = q_1$; and $q'(u_1) = 0$, where E_0 is the initial stiffness. The resulting values are

$$\alpha_1 = E_0/E_1; \quad \alpha_2 = -\text{Ln}(1/\alpha_1); \quad \alpha_3 = 1/\alpha_2 \quad (7a-c)$$

where $E_1 = q_1/u_1$ is the secant modulus to the peak point.

2. The descending branch, starting from the peak (u_1, q_1), whose equation is

$$q = q_1 \beta_1 \exp(-\beta_2 (\bar{u} - 1)^{\beta_3}) + q_{fu}; \quad \bar{u} > 1 \quad (8a,b)$$

The three parameters β_1 , β_2 , and β_3 are found by imposing the condition that the descending branch passes through the three points (u_1, q_1), (u_2, q_2), (u_3, q_3). The resulting values are

$$\beta_1 = 1 - q_{fu}/q_1; \quad \beta_2 = -\frac{\text{Ln}(R_2)}{(\bar{u}_2 - 1)^{\beta_3}} \quad (9a,b)$$

$$\beta_3 = \frac{\text{Ln} \left(\frac{\text{Ln}(R_2)}{\text{Ln}(R_3)} \right)}{\text{Ln} \left(\frac{\bar{u}_2 - 1}{\bar{u}_3 - 1} \right)} \quad (9c)$$

where $R_i = q_i - q_{fu}/q_1 - q_{fu}$ and $\bar{u}_i = u_i/u_1$, $i = 2, 3$. The two points (u_2, q_2) and (u_3, q_3) on the descending branch are shown in Fig. 2 and correspond to the following bond forces: $q_2 = 0.95q_1$ and $q_3 = 1.05q_{fu}$. u_2 and u_3 control the shape of the postpeak branch. They are input values and are selected on the basis of available experimental tests.

For the unloading path ABCD in Fig. 2, three different equations are specified. Segment AB is defined by an exponential function with initial stiffness equal to the elastic stiffness E_0 . Segment BC is described by a cubic function. Segment CD provides a smooth transition from the second segment to the reduced envelope. A second-order Bezier function is used to define the transition curve. The Bezier curve always remains between the tangents at the two end points; thus the transition curve CD can never intersect the envelope. After point D the loading path follows the reduced monotonic envelope until unloading occurs. Depending on the point where unloading or reloading occurs, different cyclic patterns can be obtained. Some of the main patterns are shown in Fig. 3. The details of these patterns and their equations are defined in Salari (1999).

Damage and degradation of the bond strength and stiffness are introduced through the reduction of the monotonic envelope, following a damage law similar to that used by Eligehausen et al. (1983) to define damage in their bond-slip law for reinforcing bars anchored in concrete. A damage function

γ is defined, where $\gamma = 0$ indicates no damage, and $\gamma = 1$ indicates full damage. The maximum slip in each direction, the difference between the peak slip values, and the number of loading cycles are the major quantities that influence the damage factor γ . These parameters can be related to the energy dissipated during the loading, unloading, and reloading cycles. In the present model the damage factor is considered a function of the total dissipated energy only. It is also assumed that only a fraction of the energy dissipated during repeated cycles between fixed peak slip values causes damage. From experimental tests it appears that the remaining energy is used to overcome the frictional resistance and is transformed into heat. Following Eligehausen et al. (1983), this fraction is assumed to be 50% of the total dissipated energy. The following expression is assumed for the damage factor:

$$\gamma = 1 - \exp(-0.1 \bar{e}_{\text{eff}}^{1.05}) \quad (10)$$

where \bar{e}_{eff} is the normalized effective hysteretic energy defined as $\bar{e}_{\text{eff}} = e_{\text{eff}}/u_1 q_1$, where $e_{\text{eff}} = 1/2 \int u q du$. The loading envelope is reduced by applying the damage factor to E_0 , q_1 , q_{fu} , and q_f .

In order to validate the performance of the proposed cyclic bond model, the experimental results obtained from two different push-pull tests are employed. The tests were carried out by Bursi and Gramola (1999) as part of research on the cyclic behavior of headed shear studs. Experimental and numerical results are shown in Figs. 4 and 5 for two different imposed slip histories. The displacement histories of the two tests are

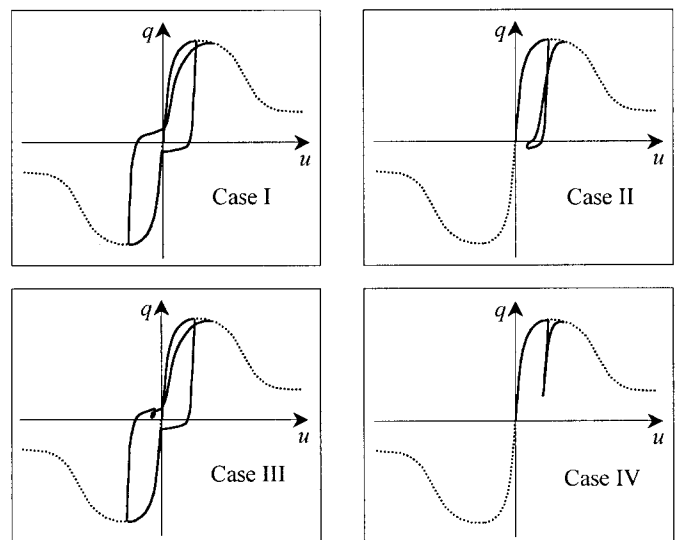


FIG. 3. Possible Unloading/Reloading Patterns

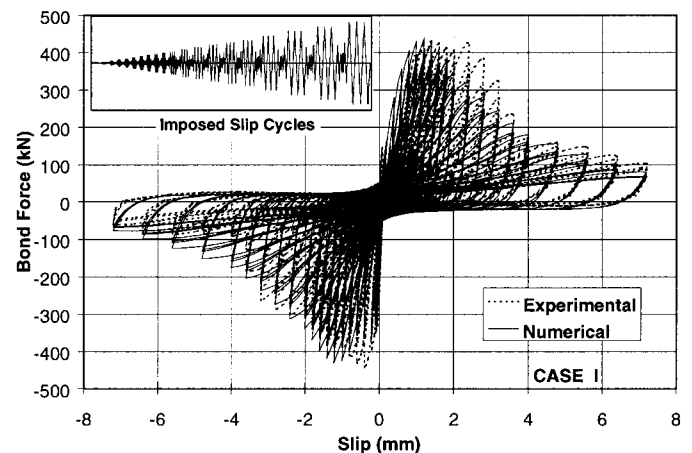


FIG. 4. Comparison of Proposed Bond Model with Experimental Results by Bursi and Gramola (1999) for Displacement History Case I

TABLE 1. Material Properties of Bond Monotonic Envelope for Correlation Studies with Experimental Data by Bursi and Gramola (1999)

Initial bond stiffness	Ultimate bond force and corresponding slip	Bond slip corresponding to $q_2 = 0.95q_1$	Bond slip corresponding to $q_3 = 1.05q_{fu}$	Frictional bond resistance
$E_0 = 1,200 \text{ kN/mm}$	$q_1 = 550 \text{ kN}$ $u_1 = 2.25 \text{ mm}$	$u_2 = 5 \text{ mm}$	$u_3 = 20 \text{ mm}$	$q_{fu} = 150 \text{ kN}$ $q_f = 20 \text{ kN}$

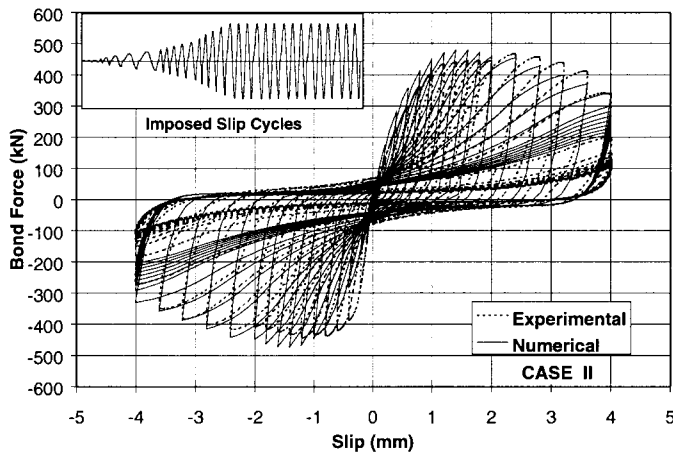


FIG. 5. Comparison of Proposed Bond Model with Experimental Results by Bursi and Gramola (1999) for Displacement History Case II

schematically shown in both figures. The first load history consists of a series of three cycles of increasing slip amplitude (up to 7 mm), and the second consists of a series of cycles of increasing amplitude up to 4 mm, followed by several cycles of constant amplitude. The material properties required to define the bond monotonic envelope are given in Table 1. The numerical results correlate well with the experimental responses. It should be pointed out that the experimental data is non-symmetric, even in the initial cycles, due to irregularities in the specimens and to minor reading problems in the actual testing. After several cycles the analytical strength degradation is close to the experimental one in Fig. 4, while the match is less satisfactory in Fig. 5. The overall good correlation between analytical and experimental results indicates that the proposed bond model can be successfully used to predict the nonlinear cyclic behavior of shear stud connections with strength and stiffness degradation.

APPLICATIONS OF STEEL-CONCRETE COMPOSITE BEAM MODEL

The performance of the force-based steel-concrete composite beam element is studied through two applications: (a) the analysis of an experimentally tested moment-resisting steel frame subassembly with a composite deck; and (b) the study of a three-story, four-bay steel frame with composite decks. All the analyses are performed with the finite-element analysis program (FEAP) (Taylor 1999). The mechanical properties of the distributed bond are calculated by smearing the strength and stiffness of a single row of shear studs over a length equal to the stud spacing.

Composite Frame Subassembly

The first application of the steel-concrete frame element is the study of the moment-resisting frame subassembly of Fig. 6. Bursi and Gramola (2000) performed a series of experimental tests on the frame under cyclic loading conditions. Their experimental investigation was supported by finite-element analyses that used solid elements for the girder and the slab and concentrated springs for the shear studs.

The steel girder has the European profile IPE330, and the

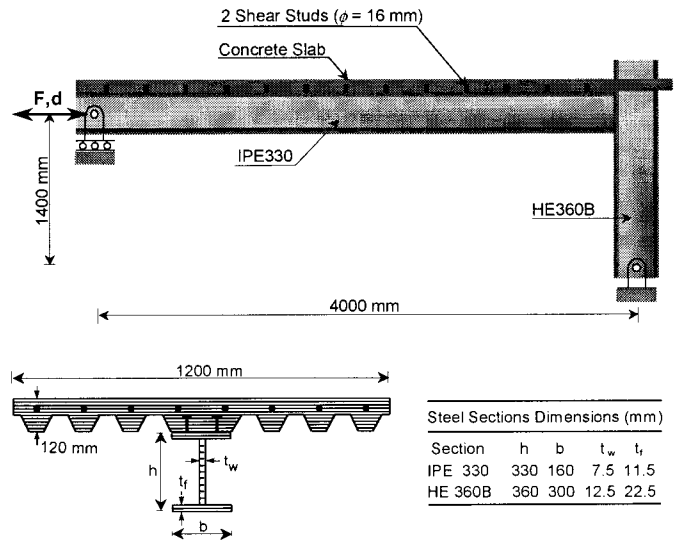


FIG. 6. Geometry and Layered Section of Moment-Resisting Frame Subassembly Tested by Bursi and Gramola (2000)

HE360B profile is used for the steel column. The cross-section characteristics and the discretization of the section into layers are given in Fig. 6. A large column section is used to induce failure in the composite beam. The slab reinforcement consists of eight $\varnothing 12$ mm rebars. This reinforcement was doubled near the column to obtain a rigid beam-to-column connection. The steel deck consists of a 0.7 mm sheet. Because of the shear lag phenomenon, one needs to consider the effective width of the concrete slab for a 2D analysis of the slab-girder systems. The effective width obtained by Bursi and Gramola (2000) with a 3D linearly elastic finite-element analysis is used in the numerical simulations. The effective width is approximately 300 mm at the left support and 500 mm at the beam-to-column connection and reaches a maximum of 900 mm at midspan. The profile of the effective width used in the analyses is found in Salari (1999).

At the beam-to-column connection, the steel beam degrees of freedom are rigidly connected to the steel column degrees of freedom. Furthermore, at this point slip in the shear connection is prevented by imposing a constraint to the slab degrees of freedom.

Two different frames were tested by Bursi and Gramola (2000). The first case considers the frame behavior with full connection, and the second deals with a frame with partial connection. The degree of shear connection, as defined by Bursi and Gramola (2000), is based on the Eurocode 4 (1992) provisions. Based on this code, two $\varnothing 16$ mm Nelson studs are placed at 200 mm intervals for full shear connection, and for the partially connected beam, a 400 mm spacing is considered. The equivalent distributed strength and stiffness are calculated by simply dividing the strength and stiffness of a single row of studs by the stud spacing. The material properties used in this analytical study are given in Table 2.

The experimental and numerical load-displacement diagrams for the frame with the fully connected beam are shown in Fig. 7. To capture the nonlinear response of the frame, only one force-based element was used. It can be observed that the numerical results agree very closely with the experimental

TABLE 2. Material Properties for Frame Subassembly by Bursi and Gramola (2000)

Full Connection			Partial Connection		
Concrete	Steel	Bond	Concrete	Steel	Bond
$f'_c = 39$ MPa $\epsilon_u = 0.003$	Girder	$E_0 = 1,640$ N/mm $q_1 = 700$ N/mm $q_{fu} = 200$ N/mm	$f'_c = 36.8$ MPa $\epsilon_u = 0.0025$	Girder	$E_0 = 820$ N/mm $q_1 = 350$ N/mm $q_{fu} = 100$ N/mm
	Rebar			Rebar	
	$f_y = 300$ MPa $E_0 = 2.05 \times 10^5$ MPa			$f_y = 300$ MPa $E_0 = 2.05 \times 10^5$ MPa	
	$f_y = 480$ MPa $E_0 = 2.1 \times 10^5$ MPa	$u_1 = 2.25$ mm $u_2 = 5$ mm $u_3 = 40$ mm $q_f = 40$ N/mm		$f_y = 480$ MPa $E_0 = 2.1 \times 10^5$ MPa	$u_1 = 2.25$ mm $u_2 = 5$ mm $u_3 = 40$ mm $q_f = 20$ N/mm

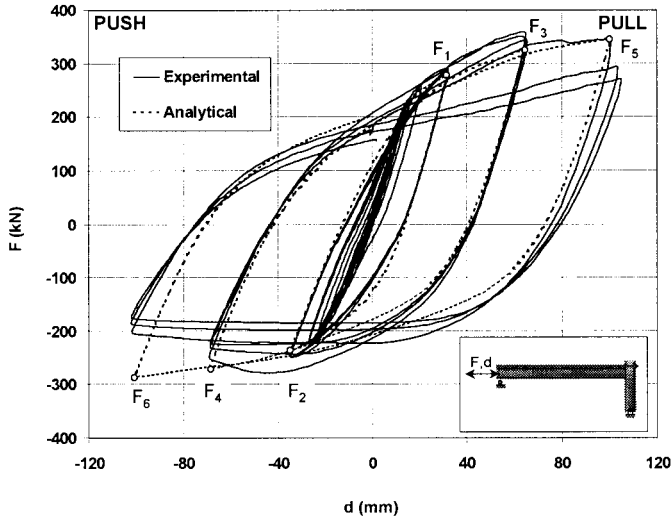


FIG. 7. Load-Displacement Diagram for Fully Connected Frame

ones for the positive lateral load, for which the concrete slab is essentially under compression. When the lateral load is negative and the concrete slab is under tension, the experimental results show some discrepancies in the larger cycles, due the gradual loss of strength observed in the experiment, caused by local buckling in the steel beam. This phenomenon is not captured by the proposed composite beam element, which neglects geometric nonlinearities.

The “exact” analytical bond force distributions along the composite beam with full connections are shown in Fig. 8. The six distributions (labeled F1 through F6) correspond to the loading points indicated in Fig. 7. These results were obtained using a very large number of displacement-based composite elements with partial connection. The drop in the bond force near the beam-to-column connection at load points F3 and F5 follow the crushing of the slab concrete in compression. The drops in the bond force at approximately 3,000 mm from the left support at load points F4 and F6 follow tension yielding of the steel reinforcement in the slab. This drop appears at approximately 3,000 mm from the left support because at this point some of the reinforcement placed around the beam-to-column connection is interrupted. Yielding of the slab reinforcement near the beam end causes a similar bond drop at load point F6. The bond force distributions obtained with a single force-based element are presented in Fig. 9. Even though these distributions are obtained with a single force-based element for the composite beam, they are in good agreement with the analytical results. The discrepancy at the right node of the beam is due to the fact that slip is prevented at the beam-to-column connection. The jump in the bond force distribution at the end of the composite beam is typical of force-based elements, where bond force continuity is not enforced. The discontinuity has no significant effect on the overall response of the frame.

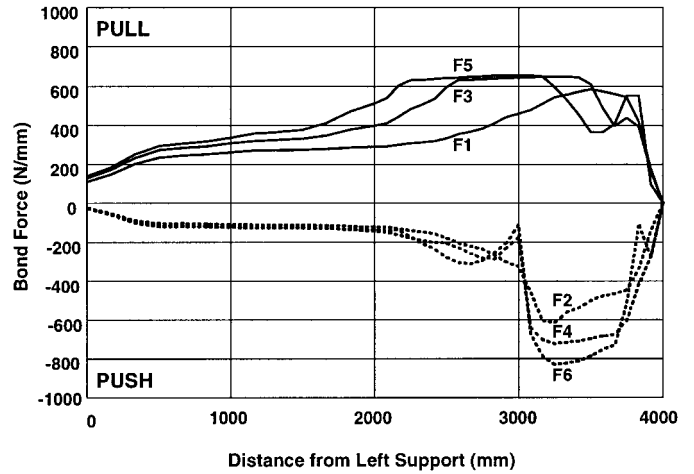


FIG. 8. “Exact” Analytical Bond Force Distributions along Fully Connected Beam

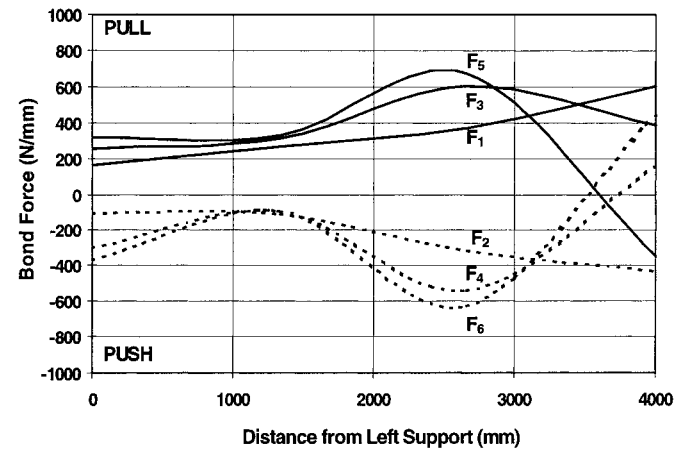


FIG. 9. Bond Force Distributions along Fully Connected Beam with One Force-Based Element

The experimental and numerical load-displacement diagrams for the frame with the partially connected beam are shown in Fig. 10. The nonlinear response of the frame was captured with only one force-based element. Similar to the previous case, the numerical results agree with the experimental results for the positive lateral load, for which the concrete slab is essentially under compression. When the lateral load is negative, the experimentally observed local buckling in the steel girder is not captured by the proposed model. The main source of nonlinearity in the force-displacement responses of Fig. 10 is the yielding of the steel girder.

The “exact” analytical bond force distributions along the composite beam with partial connections at different displacement levels are shown in Fig. 11, while the bond force distribution obtained with one element is shown in Fig. 12. The six distributions (labeled P1 through P6) correspond to the loading

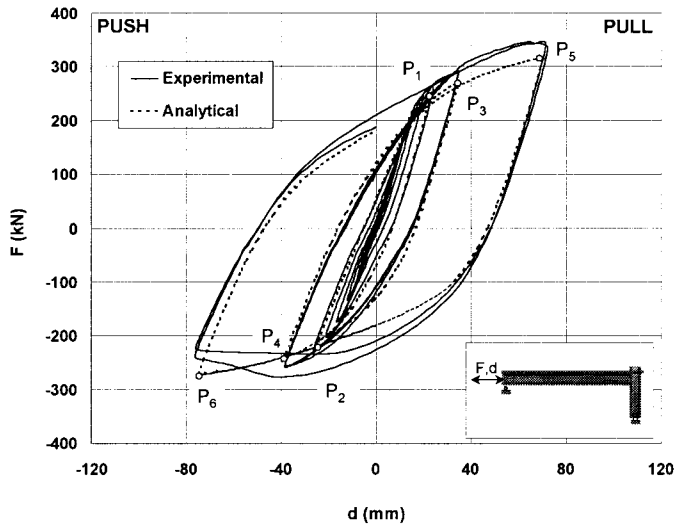


FIG. 10. Load-Displacement Diagram for Partially Connected Frame

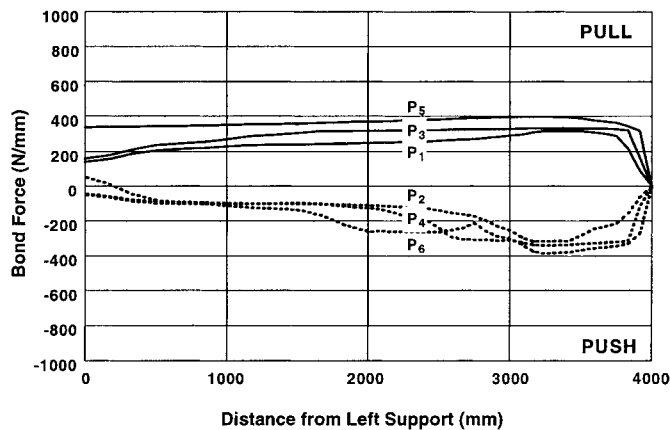


FIG. 11. "Exact" Analytical Bond Force Distribution along Partially Connected Beam

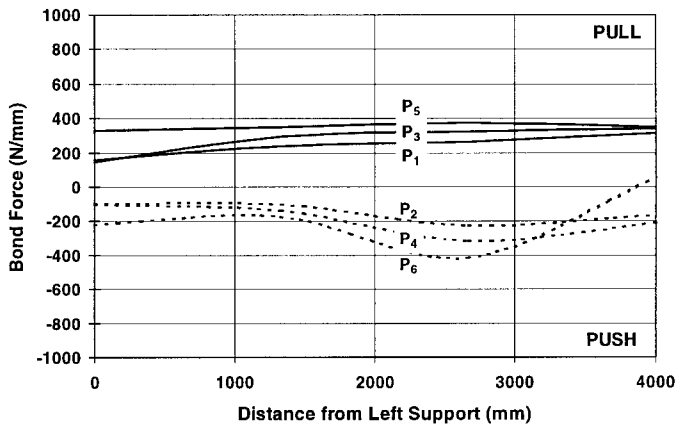


FIG. 12. Bond Force Distribution along Partially Connected Beam with One Force-Based Element

points indicated in Fig. 10. The agreement between analytical and experimental distribution is good, with the aforementioned discrepancy at the beam-to-column connection. The bond force distribution in the case of partial connections is smoother than in the case of full connection because the lower level of connection leads to a lower composite action and thus to smaller strains in the reinforced concrete slab. Finally, no shear connection failure was observed in either of the two examples.

Three-Story Composite Frame

This application deals with the nonlinear response of the composite frame of Fig. 13 under the lateral and vertical loads of Fig. 14. The steel frame of the composite system is the three-story Seattle building studied by Stojadinovic et al. (1998) in the framework of the SAC Steel Project that followed the 1994 Northridge earthquake. Stojadinovic et al. (1998) performed a series of pushover analyses to study the sensitivity of the frame response to different degrees of base column connection. The concrete slab was included in the load analysis by Stojadinovic et al. (1998), but it was not considered as part of the structural load-resisting system. The same system is considered here, but the composite slab is an integral part of the structural system. The base columns are considered fixed. Full shear connection between the concrete slabs and the steel girders is provided by two 12.7 mm diameter studs spaced at 150 mm along the girders. The material properties are given in Table 3. A design base shear of $V_{UBC} = 373$ kN was obtained for the steel frame by Stojadinovic et al. (1998). The lateral load distribution used in the pushover analyses is

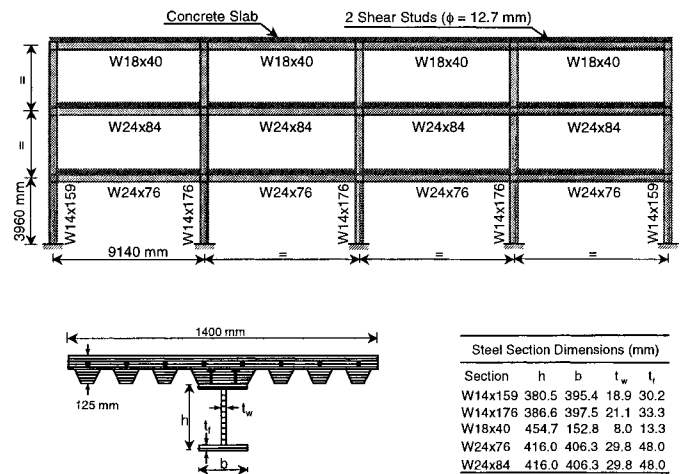


FIG. 13. Characteristics of Composite Frame

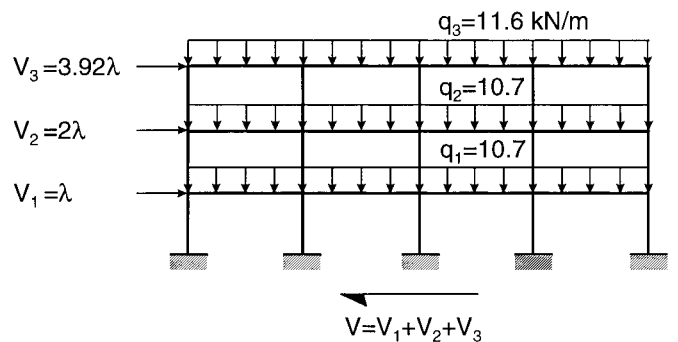


FIG. 14. Loading Condition for Composite Frame

TABLE 3. Material Properties for Three-Story Steel Frame with Composite Girder

Full Connection		
Concrete	Steel	Bond
	Girder	
$f'_c = 28$ MPa	$f_y = 345$ MPa	$E_0 = 1,860$ N/mm
$\epsilon_u = 0.003$	$E_0 = 2.0 \times 10^5$ MPa	$q_1 = 700$ N/mm
		$q_{fu} = 150$ N/mm
	Rebar	
	$f_y = 345$ MPa	$u_1 = 2.25$ mm
	$E_0 = 2.0 \times 10^5$ MPa	$u_2 = 5$ mm
		$u_3 = 40$ mm

based on the Uniform Building Code (ICBO 1997) and is shown in Fig. 14.

The frame is analyzed using two force-based composite beam elements per beam. Due to the kinematics of the composite beam element, the finite-element model has two horizontal degrees of freedom at each node, one in the steel beam and the other in the concrete slab. In the frame model, the steel girder is rigidly connected to the steel column. The horizontal degrees of freedom of the concrete slabs are connected only to those of the adjacent concrete slabs (in the interior connections) or are free (at the girder ends). The steel columns are modeled using a single force-based fiber element with material nonlinearities. Nonlinear geometric effects are neglected in the columns. The uniform distributed loads on the beams are applied as equivalent nodal loads. The distributed loads are applied at the first load step and remain constant during the pushover analyses.

The application of the floor loads indicated in Fig. 14 poses an interesting problem. The lateral load distribution computed from the Uniform Building Code (ICBO 1997) is a series of concentrated loads applied at each floor, but the floor model has two horizontal degrees of freedom: one in the steel girder and the other in the concrete slab. The lateral load at each floor level can either be divided between the two horizontal degrees of freedom or solely applied to one of them. The writers observed that when the lateral load at each floor level is equally divided between the two degrees of freedom, the predicted frame capacity increases by about 5% with respect to the case where the entire lateral load is applied to the steel girders. This is due to the fact that if the load is split between girder and slab, the entire girder carries the lateral load, while in the other case the load applied to the steel girder is gradually transferred to the concrete slab, thus overloading the end steel girders. The results presented hereafter distribute the loads equally between the steel girder and the concrete slab because it is believed that the lateral forces are carried directly by the composite beams.

The normalized base shear V/V_{UBC} versus the roof drift Δ/H for different levels of shear connection are shown in Fig. 15, where H is the total height of the frame. The case of the steel frame with no concrete slab is also included. The degree of shear connection is defined by the parameter μ ; $\mu = 1$ indicates full connection (which implies that additional shear studs do not increase the strength of the beam), while $\mu = 0$ indicates no connection. Fig. 15 shows how replacing the steel girder with the steel-concrete composite beams increases the initial stiffness of the steel frame. Similarly, the strength of the frame increases by approximately 25%, depending on the degree of connection.

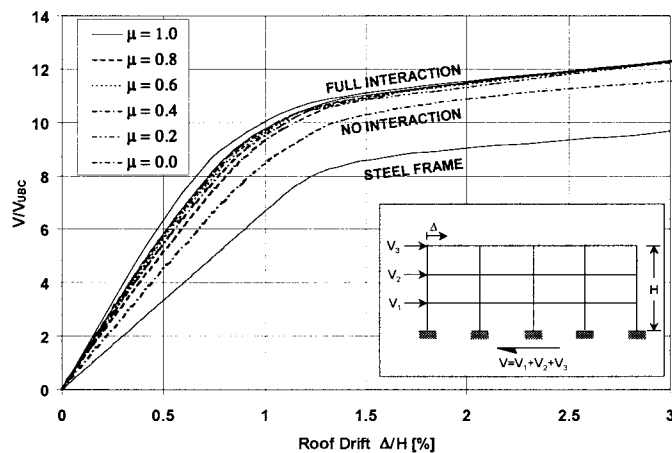


FIG. 15. Load-Displacement Diagrams for Different Levels of Shear Connections

It is, however, interesting to observe that the stiffness and strength of the building do not drastically change for degrees of connection that vary from $\mu = 0.2$ to $\mu = 1$, thus indicating that an analysis with no slip between steel girder and concrete slab provides, in most cases, a good approximation of the frame strength. This result was validated by a series of parametric studies on steel frames with composite slabs performed by Salari (1999). Finally, the results confirmed that the design of the original SAC building, based on the Uniform Building Code (ICBO 1997), gives a very large building overstrength (eight for the steel frame without the concrete slab, ten for the composite frame).

SUMMARY AND CONCLUSIONS

The application of a recently developed steel-concrete composite beam element to the study of steel frames with composite slabs is discussed in this paper. The steel-concrete composite beam stems from a force-based formulation and can model the highly nonlinear response of composite beams, including concrete crushing and shear stud failure, without numerical problems. The original composite element is enhanced by the development of a new nonlinear law for modeling the behavior of the shear stud connections. The law is fully cyclic and includes stiffness and strength degradation during the load cycles. The model parameters are determined by fitting a series of push-pull experimental tests on shear studs. The model can reproduce the salient characteristics of the cyclic experimental responses.

Two applications are presented to illustrate the performance of the force-based element and to show the importance of the composite action in composite frames. The first application presents two composite subassemblies tested at the University of Trento, Italy. Even though only one force-based element is used to model the composite beam, the force-displacement responses are in close agreement with the experimental results. Even though the bond-stress distribution along the beam is somehow approximate, the overall results are very good. The failure mechanism of the subassembly, due to local buckling of the steel girder, cannot be captured by the composite beam model, which does not include geometric nonlinearities.

The second application extends the composite beam element to the study of a full-scale steel frame with a steel-concrete composite deck. The steel frame was previously studied while neglecting the contribution of the composite action. As expected, the overall response of the frame is greatly enhanced by the composite deck, which increases both the stiffness and the strength of the frame. Different levels of connection in the composite beams have little effect on the overall response, which seems to remain almost unchanged for degrees of connection larger than 20% of that of the full connection. Because of the considerable increase in the initial stiffness in the frame due to the composite action, this action should be included in computing the fundamental period of the structure, which is used to find the seismic design forces for the frame.

All the analyses discussed in this study were performed in a matter of minutes on a personal computer. The precision of the proposed composite beam element reduces the number of elements needed to discretize the composite members, thus drastically reducing the computational cost of the frame analysis. Continuous advances in computer architecture, combined with accurate models such as the one presented in this paper, make nonlinear frame analysis a realistic tool for assessing the response of structural frames within the framework of the emerging performance-based engineering philosophy. Future analytical studies on composite frames should combine models for the composite members with models for the beam-to-column connections, whose deformability has an important im-

pact on the overall frame stiffness, especially at large levels of lateral displacements.

ACKNOWLEDGMENTS

This work was supported by the National Science Foundation under Grant No. CMS-9520282. This support is gratefully acknowledged. The opinions expressed in this paper are those of the writers and do not necessarily reflect those of the sponsor. The writers would also like to thank Prof. P. B. Shing and D. M. Frangopol of the University of Colorado for their valuable insight in the early stages of the research and Prof. R. L. Taylor of the University of California, Berkeley, for his continuous efforts to enhance program FEAP. Special thanks go to Prof. O. Bursi of the University of Trento, Italy, for providing the experimental test data.

REFERENCES

- Amadio, C., and Fragiaco, M. (1993). "A finite element model for the study of creep and shrinkage effects in composite beams with deformable shear connections." *Costruzioni Metalliche*, 4, 213–228.
- Ayoub, A., and Filippou, F. C. (2000). "Mixed formulation of nonlinear steel-concrete composite beam element." *J. Struct. Engrg.*, ASCE, 126(3), 371–381.
- Bursi, O. S., and Gramola, G. (1999). "Behaviour of headed stud shear connectors under low-cycle high amplitude displacements." *Mat. and Struct.*, Paris, 32, 290–297.
- Bursi, O. S., and Gramola, G. (2000). "Behaviour of composite substructures with full and partial shear connection under quasi-static cyclic and pseudo-dynamic displacements." *Mat. and Struct.*, Paris, 33, 154–163.
- Daniels, B. J., and Crisinel, M. (1993). "Composite slab behavior and strength analysis. Part I: Calculation procedure." *J. Struct. Engrg.*, ASCE, 119(1), 16–35.
- Eligehausen, R., Popov, E. P., and Bertero, V. V. (1983). "Local bond stress-strain relationships of deformed bars under generalized excitations." *Rep. UCB/EERC-82-23*, Earthquake Engrg. Res Ctr., University of California, Berkeley.
- El-Tawil, S., Kanno, R., and Deierlein, G. G. (1996). "Inelastic models for composite moment connections in RCS frames." *Composite construction in steel and concrete III*, C. D. Buckner and B. Shahrooz, eds., ASCE, New York, 197–210.
- European Committee for Standardization (Eurocode 4). (1992). "Design of composite steel and concrete structures. Part 1-1: General rules and rules for buildings." *ENV 1994-1-1*, Brussels.
- Hajjar, J. F., Schiller, P. H., and Molodan, A. (1998). "A distributed plasticity model for concrete-filled steel tube beam-columns with interlayer slip." *Engrg. Struct.*, 20(8), 663–676.
- International Conference of Building Officials (ICBO). (1997). *Uniform building code*, Vol. 2, Whittier, Calif.
- Kent, D. C., and Park, R. (1971). "Flexural members with confined concrete." *J. Struct. Div.*, ASCE, 97(7), 1964–1990.
- Menegotto, M., and Pinto, P. E. (1973). "Method of analysis for cyclically loaded reinforced concrete plane frames including changes in geometry and nonelastic behavior of elements under combined normal force and bending." *IABSE Symp. on Resistance and Ultimate Deformability of Struct. Acted on by Well-Defined Repeated Loads*, International Association for Bridge and Structural Engineering, Zurich, 112–123.
- Salari, M. R. (1999). "Modeling of bond-slip in steel-concrete composite beams and reinforcing bars." PhD thesis, Dept. of Civ., Envir. and Arch. Engrg., University of Colorado, Boulder.
- Salari, M. R., and Spacone, E. (2001). "Finite element formulations of one-dimensional elements with bond-slip." *Engrg. Struct.*, 23(7), 815–826.
- Salari, M. R., Spacone, E., Shing, P. B., and Frangopol, D. M. (1998). "Nonlinear analysis of composite beams with deformable shear connectors." *J. Struct. Engrg.*, ASCE, 124(10), 1148–1158.
- Spacone, E., Filippou, F. C., and Taucer, F. F. (1996). "Fiber beam-column model for nonlinear analysis of R/C frames. I: Formulation, II: Applications." *Earthquake Engrg. and Struct. Dyn.*, 25(7), Part I, 711–725, Part II, 726–742.
- Stojadinovic, B., Spacone, E., Goel, S. C., and Kwon, M. (1998). "Influence of semi-rigid base models on the response of steel MRF buildings." *6th U.S. Nat. Conf. on Earthquake Engrg.*, Earthquake Engineering Research Institute, Oakland, Calif. (CD-ROM).
- Taylor, R. L. (1999). *FEAP User Manual, Version 7.1*. Dept. of Civ. and Envir. Engrg., University of California, Berkeley. (<http://www.ce.berkeley.edu/~rlt/feap/>).

NOTATION

The following symbols are used in this paper:

- $D_b(x)$ = bond force/unit length;
 \mathbf{e} , \mathbf{e}_b = main body and bond deformations;
 \mathbf{F} , \mathbf{K} = element flexibility and stiffness matrices, respectively;
 \mathbf{F}_{BB} , \mathbf{F}_{Bb} , \mathbf{F}_{bB} , \mathbf{F}_{bb} = element flexibility terms;
 \mathbf{f} , \mathbf{f}_b = main body and bond flexibility;
 \mathbf{N}_{BB} , \mathbf{N}_{Bb} , \mathbf{N}_{bB} , \mathbf{N}_{bb} = force interpolation functions;
 \mathbf{Q} , \mathbf{Q}_b = element and bond generalized forces;
 q , u = bond force and bond slip;
 \mathbf{s} , \mathbf{s}_b = main body and bond forces;
 \mathbf{U} , \mathbf{U}_B , \mathbf{U}_b = nodal displacements, main body, and bond contributions;
 α_1 , α_2 , α_3 , β_1 , β_2 , β_3 = bond law parameters; and
 γ = damage factor.